Characterization of Silicon Electro-Optical Modulator for Analog Optical Links

Xianshu Luo, Junfeng Song, Xiaoguang Tu, Tsung-Yang Liow, Qing Fang, Mingbin Yu, and Guo-Qiang Lo

***Abstract*—We investigate the analog performances of a silicon Mach-Zehnder interferometer electro-optical modulator. We characterize the optical responses upon various DC and RF voltage supplies. We also measured the spur-free dynamic range (SFDR) of the modulator using two-tone method, showing maximum SFDR of 40 dBc and 46 dBc respectively for second harmonic distortion and third-order intermodulation distortion.**

***Index Terms*—MZI modulator, slope efficiency, spur-free dynamic range, silicon integrated device.**

I. Introduction

RF-/Microwave-photonics [1]-[2] has gained widespread applications to analog optical links such as radio-over-fiber, phase-arrayed antenna, antenna remoting for radar systems, subcarrier transmission, etc. As one of the basic building blocks in microwave photonic links, optical modulator plays an important role for the E/O conversion. In order to determine the performance of an E/O conversion, several performance metrics are considered for an optical modulator, including the modulation efficiency, the RF gain, and the nonlinearity [3]. While the modulation efficiency can be determined by measuring the half-wave voltage, the RF gain is characterized by measuring the slope efficiency (SE) and the nonlinearity is determined by measuring the spur-free dynamic range (SFDR). Previous work has shown the characterization of such parameters for III-V electro-absorption modulators [4]-[5]. Meanwhile, the unprecedented growth of the silicon photonics has driven the development of silicon-based electro-optical modulators using free-carrier dispersion effect [6]. High-speed silicon modulators have been demonstrated over the past few years [7]-[12]. However, only few work focused on the characterization of the silicon modulator for RF links [13], while most of the demonstrations focused on the optical performance for telecommunication applications, pursuing high modulation speed and low power consumption [7]-[12].

Manuscript received June 6, 2012; revised August 31, 2012.

This work was supported by the Science and Engineering Research Council of A*STAR (Agency for Science, Technology and Research), Singapore under SERC grant number: 102 174 0174.

Xianshu Luo, Junfeng Song, Xiaoguang Tu, Tsung-Yang Liow, Qing Fang, Mingbin Yu, and Guo-Qiang Lo are with the Institute of Microelectronics, A*STAR (e-mail: luox@ime.a-star.edu.sg)

Junfeng Song is also with State Key Laboratory on Integrated Opto-Electronics, College of Electronic Science and Engineering, Jilin University, Changchun, People's Republic of China, 130021.

II. Device Characterization

The silicon MZI modulator investigated here is with the same design to our previous demonstrations [12]. The waveguide height is 220 nm with 60 nm slab. The waveguide width is 0.6 μm. The length of the phase shift is 4 mm.

A. *Slope Efficiency*

The slope efficiency is an important parameter for analog application. It can be obtained by plotting the output power of the modulator against the driving voltage. High slope efficiency suggests a high link gain. We first investigate the slope efficiency via measuring the optical transmission responses upon different DC bias. We use a broadband amplified spontaneous emission (ASE) as the light source and an optical spectrum analyzer (OSA) to collect the transmission spectra. Fig. 1(a) shows the normalized optical intensities as functions of the applied DC bias at the quadrature point of 1563.0 nm. As the increase of the reverse bias, the optical intensity decreases due to the resonance shift. The slope efficiency can then be extracted from the variation of the optical intensity. Figure 1(b) shows the extracted slope efficiency with different bias. The maximum slope efficiency is ~ 0.4 V^{-1} with small bias.

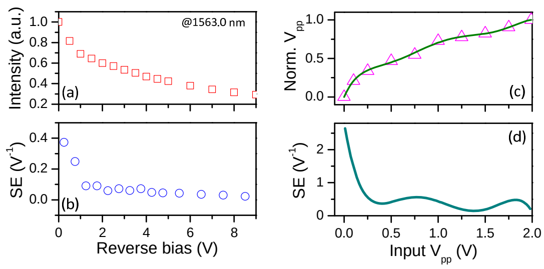

Fig. 1. (a) The optical intensities and (b) the extracted slope efficiency at 1563.0 nm upon different reverse bias. (c) The normalized Vpp of the output signals and the (d) extracted slope efficiency upon different Vpp of the input signals.

We also investigate the slope efficiency of the silicon MZI modulator upon RF signal driving with different peak-to-peak voltages, VPPs. The carrier wavelength is selected at the quadrature point of 1563.0 nm. We gradually increase the RF signal VPP from 0V to 2V, which is limited by the signal generator. We read the optical output signal from the oscilloscope and compare the output Vpp at different input VPPs. We fix the input signal of 50 MHz during the measurements. Figure 1(c) shows the output Vpp with different input Vpp, which is normalized to the maximum output Vpp. The output RF power non-linearly increases as the increase of the input RF power. Similarly, we can extract the slope efficiency and plot in Fig. 1(d). The maximum slope efficiency upon RF drive is ~ 2.5 V-1 at

DOI: 10.7763/IJIEE.2012.V2.231

small input signal. Both DC and RF measurements suggest that it is better to work with small RF signal with small bias voltage in order to obtain high slope efficiency.

B. *Spur-Free Dynamic Range*

Spur-free dynamic range (SFDR) is another critical parameter for modulators in analog application for the characterization of the nonlinearities. It is defined as difference in the RF input in the link between the signal level that produces an output equal to the noise level and the signal level that would produce distortion products equal to the noise level. Due to the optical non-linearity, in addition to the carrier, there will be second harmonic distortion (SHD), third harmonic distortion (THD), third-order inter-modulation distortion (IMD3), and other higher order nonlinear terms in the output RF signal. Such distortions can be measured by using the two-tone method. Fig. 2 conceptually illustrates the frequency components generated during the two-tone method. The two input carriers are with the frequencies of f1 and f2. The high-order harmonics appear at the frequency of the multiple times of the carrier frequency, e.g. 2f, 3f, etc., while the IMD3 products appear at the frequencies of 2f2-f1 and 2f1-f2. The narrow-band system is mostly affected by the IMD3 products as they fall within the band while the other distortion products are out of band. In the following part, we will investigate both IMD3 and SHD.

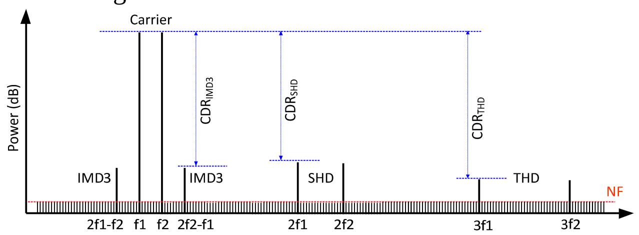

Fig. 2. Illustration of the high-order harmonics generated due to the optical non-linearity. IMD3: 3rd order intermodulation distortion, CDR_{IMD3}: carrier-to-third-order intermodulation distortion ratio, SHD: Second-order harmonic distortion, CDR_{SHD}: carrier-to-second-order harmonic distortion ratio, THD: third-order harmonic distortion, CDR_{THD}: carrier-to-third-order harmonic distortion ratio, NF: noise floor.

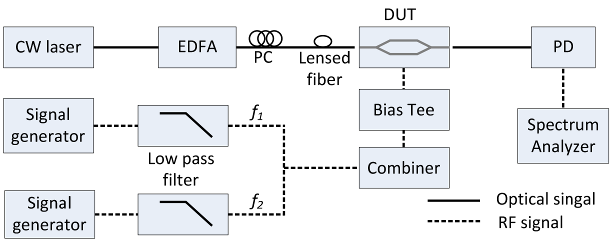

Fig. 3. Block diagram of the two-tone measurement setup. EDFA: erbium-doped fiber amplifier, PC: polarization controller, DUT: device under test, PD: photodiode.

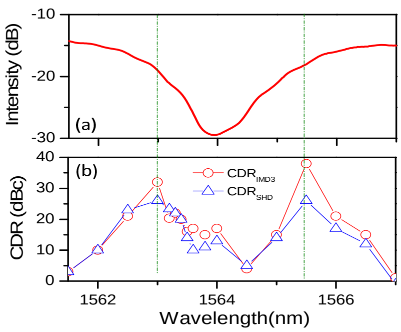

Fig. 4. The dependence of the CDR on the wavelengths.

Fig. 3 shows the block diagram of the two-tone measurement setup. A CW laser sitting at certain wavelength is endfire to an EDFA in order to boost up the optical power to overcome the total link loss. Two RF signals with frequency of 50 MHz and 50.1 MHz are generated using two identical signal generators and combined by a high-speed power combiner after low-pass filters. A bias tee is inserted in order to bias the input signal. The output optical signal is detected by a high-speed (40 GHz) photodiode and collected by spectrum analyzer. The input RF powers for the two tones can be read from the signal generator while the output electrical powers for the four harmonics at 49.9 MHz, 50 MHz, 50.1 MHz, and 50.2 MHz can be directly read from the spectrum analyzer.

Fig. 4(a) shows the transmission spectra while Fig. 4(b) shows the measured CDR dependence on the wavelength. The CDRs are measured with the DC bias of 3.5 V and the two-tone electrical powers of 12 dBm. For both CDR_{IMD3} and CDR_{SHD}, the results clearly show the wavelength dependence with the maximum CDRs appear at the quadrature point and the minimum at the resonance wavelength. This suggests the importance of the working wavelength selection. The maximum CDR_{IMD3} and CDR_{SHD} are ~ 40 dBc and 25 dBc.

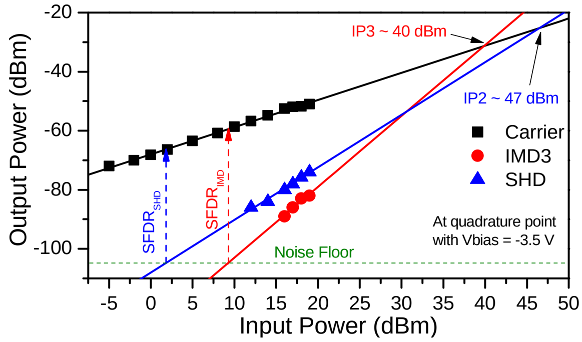

Fig. 5. The power dependences of the carrier, IMD3 and SHD as functions of the input RF power. The SFDRs and the intercept points are extracted from the plot for both IMD3 and SHD.

With fixed carrier wavelength of 1563.0 nm and bias voltage of 3.5 V, we characterize the device SFDR by measuring the power changes of each frequency component upon different input RF powers of the two tones. Fig. 5 shows the measured frequency component powers as functions of the input two-tone powers. All of them linearly increase as the increase of the two-tone powers. Based on the SFDR definition, we can extract them for both IMD3 and SHD as shown inf Fig. 5. The $SFDR_{IMD3}$ and $SFDR_{SHD}$ are respectively 46 dBc and 40 dBc. Furthermore, we can extract the intercept point (IP) which is defined as the input power at which a linear fit of the two measurements cross. From the measurements, the IP3 and IP2 are respectively 40 dBm and 47 dBm, suggesting the demonstrated MZI modulator is with tolerance to the affects from both IMD3 and SHD.

III. Conclusion

We investigate the analog performances of a silicon Mach-Zehnder interferometer electro-optical modulator. We characterize the optical responses upon various DC and RF voltage supplies. We also measured the spur-free dynamic range (SFDR) of the modulator using two-tone method, showing maximum SFDR of 40 dBc and 46 dBc respectively for second harmonic distortion and third-order intermodulation distortion.

ACKNOWLEDGMENT

This work was supported by the Science and Engineering Research Council of A*STAR (Agency for Science, Technology and Research), Singapore under SERC grant number: 102 174 0174. Xianshu Luo acknowledges the discussion with Dr. Lim Peng Huei.

REFERENCES

[1] J. Capmany, B. Ortega, and D. Pastor, "A Tutorial on Microwave Photonic Filters," *J. Lightwave Technol*, vol. 24, pp. 201-229

[2] R. A. Minasian, "Photonic Signal Processing of Microwave Signals," *IEEE Transactions on Microwave Theory and Techniques*, vol. 54, pp. 832-846, 2006.

[3] S. Iezekiel, "Measurement of microwave behavior in optical links," *IEEE microwave magazine*, pp. 100-120, 2008.

[4] R. B. Welstand, S. A. Pappert, D. T. Nichols, L. J. Lembo, Y. Z. Liu, and P. K. L. Yu, "Enhancement in electroabsorption waveguide modulator slope efficiency at high optical power," *IEEE Photon. Technol*. Lett. 10, pp. 961 – 963, 1998.

[5] B. Liu, J. Shim, Y. Chiu, H. F. Chou, J. Piprek, and J. E. Bowers, "Slope efficiency and dynamic range of traveling-wave multiple-quantum-well electroabsorption modulators," *IEEE Photon. Technol.* Lett. 16, pp. 590-592, 2004.

[6] R. Soref and B. Bennett, "Electrooptical effects in silicon," *IEEE J. Quantum Electron.* vol. 23, pp. 123-129, 1987.

[7] L. Liao, A. Liu, D. Rubin, J. Basak, Y. Chetrit, H. Nguyen, R. Cohen, N. Izhaky, and M. Paniccia, "40Gbit/s silicon optical modulator for high-speed applications," Electron. Lett. 43, pp. 1196-1197, 2007.

[8] J. B. You, M. Park, J. W. Park, and G. Kim, "12.5 Gbps optical modulation of silicon racetrack resonator based on carrier-depletion in asymmetric p-n diode," *Opt. Express 16*, pp. 18340-18344, 2008.

[9] D. M. Morini, L. Vivien, J. M. Fedeli, E. Cassan, P. Lyan, and S. Laval, "Low loss and high speed silicon optical modulator based on a lateral carrier depletion structure," *Opt. Express* vol. 16, pp. 334-339, 2008.

[10] F. Y. Gardes, A. Brimont, P. Sanchis, G. Rasigade, D. M. Morini, L. O'Faolain, F. Dong, J. M. Fedeli, P. Dumon, L. Vivien, T. F. Krauss, G. T. Reed, and J. Marti, "High-speed modulation of a compact silicon ring resonator based on a reverse-biased pn diode," *Opt. Express* vol. 17, pp. 21986-21991,2009

[11] T. Tanabe, K. Nishiguchi, E. Kuramochi, and M. Notomi, "Low power and fast electro-optic silicon modulator with lateral p-i-n embedded photonic crystal nanocavity," *Opt. Express*, vol. 17, pp. 22505-22513 (2009).

[12] T. Y. Liow, K. W. Ang, Q. Fang, J. Song, Y. Xiong, M. Yu, G. Q. Lo, and D. L. Kwong, "Silicon modulators and germanium photodetectors on SOI: monolithic integration, compatibility, and performance optimization," *IEEE J Selected Top. Quantum Electron.* vol. 16, pp. 307-315, 2010.

[13] F. Vacondio, M. Mirshafiei, J. Basak, A. Liu, L. Liao, M. Paniccia, and L. A. Rusch, "A Silicon Modulator Enabling RF Over Fiber for 802.11 OFDM Signals," *IEEE J. Selected Top. Quantum Electron.* vol. 16, pp. 141-148, 2010.